

On the Mathematical Treatment of Engineering Problems: Examples from the Cassini Spacecraft Attitude Control System Design

An invited paper for the 39th Workshop at the G. Stampacchia International School of Mathematics

Allan Y. Lee

Mail Stop 230-104, Jet Propulsion Laboratory, 4800 Oak Grove Drive, Pasadena, California 91109-8099, U.S.A.

1. APPLYING MATHEMATICS TO ENGINEERING PROBLEMS

1.1 Engineers need more Mathematics?

Engineering mathematics is generally considered as a collection of mathematical methods adapted for the solution of physical and engineering problems. Because of their fundamental importance, the following mathematical methods are commonly included in the mathematics curriculums of engineering schools:

- Vector differential and integral calculus,
- Solution of a system of linear equations,
- Linear system theory,
- Laplace transformation,
- Power series, Taylor and Laurent series,
- Matrices and Eigen-value problems,
- Calculus of variations and “hill-climbing” optimization techniques,
- Methods of approximation,
- Statistical methods,
- Fourier series, Fourier integrals, and Fourier transformation,
- Boolean algebra,
- Numerical solutions of ordinary and partial differential equations,
- Legendre and Chebyshev polynomials, and Bessel functions.

The list is incomplete, but even so it is quite comprehensive. Solutions to physical and engineering problems often might require lengthy numerical calculations but they seldom require the use of advanced methods of mathematical analyses. This is especially true when only an approximate solution (instead of an exact solution) to the problem in hand is all that interested the engineer/scientist involved. If this is the case, why is it often said that engineers nowadays need more and more mathematics?

1.2 Weaknesses in the Mathematical Education of Engineers

The application of mathematics to physical problems involves three stages:

- (1) Idealization of a physical situation and formulation in mathematical terms,
- (2) Manipulation of the mathematical symbolism, and
- (3) Interpretation of the solution in physical terms.

In a past survey, it was reported that the majority of engineers considered the formulation of a physical problem in mathematical terms (Step 1) the hardest step. A contributory reason may be that much mathematics teaching stresses the manipulative aspect (Step 2) at the expense of the model building aspect. Additionally, it is the observation of this author that many practicing engineers have difficulty in drawing conclusions from the mathematical solution of the problem. They also do not know how to interpret the solution in physical terms (Step 3). In other words, it seems that in many cases the amount of mathematics taught in engineering schools is quite adequate, but the ability to find the proper mathematical setup for a given physical or engineering problem is not taught to the students to a sufficient degree. Therefore, the need is not so much for "more" mathematics as for a better training in problem formulation.

If these observations are valid, steps must then be taken to improve the current state of affairs. For what good it is to be able to correctly solve an incorrectly formulated problem? In the opinion of this author, at a minimum, mathematicians who teach engineering mathematics must be aware of the engineering applications of the mathematics they teach and be prepared to present the subject in a way that the engineering students will find relevant and stimulating. To this end, the mathematicians involved must establish contact with professors from the engineering departments from which the majority of their students come. Together, they should demonstrate how a complex "real-life" engineering problem can be simplified and then solved using a mathematical method the mathematician has just introduced. The engineering staffs have the added responsibility of ensuring that students be aware of the limitations imposed on the results of a mathematical application by the assumptions imposed on the original physical situation in reducing it to a reasonable mathematical model. The relevancy between a mathematical technique and the engineering problems that the students must solve must be convincingly established.

Yet one more way to supplement the teaching of mathematics to engineering students is for practicing engineers to share their experience with their teaching colleagues. This can take the forms of invited guest speakers, published books and articles in engineering magazines, organized workshops, and others. The objective of this paper is to illustrate how common mathematical methods could be used in the effective solutions of aerospace engineering problems. To this end, we use three engineering problems that are related to the design of the Attitude and Articulation Control Subsystem (AACS) of the Cassini/Huygens spacecraft. These examples are selected because of the author's familiarity with them. They are by no mean the most important or most mathematical challenging problems. The problems addressed are:

- (1) In-flight estimation of the Cassini spacecraft's inertia tensor,
- (2) The design of a Cassini thruster leakage detection monitor, and
- (3) The design of the Cassini spacecraft pointing control system.

1.3 Huygens and Cassini: the Applied Mathematicians

The great Dutch philosopher Christiaan Huygens (1629-1695) was both a physicist and a mathematician. He invented the pendulum clock in 1656. He discovered the rings of Saturn in 1655-1656 and the largest moon of Saturn, Titan, in 1655. In his studies of mechanics, he introduced the important concepts of "*moment of inertia*" (1673) and "*centrifugal force*." He also made the first accurate determination of the value of acceleration due to gravity and showed that it varied with latitude.

In 1676, Huygens conceived his geometrical theory of wave propagation in optics. In this theory, he considered light as the effect of "waves" propagating spherically in ether. In 1678, Huygens established the *Huygens' principle of wave front propagation*. This principle recognizes that each point of an advancing wave front is in fact the center of a fresh disturbance, and the source of a new train of waves. Put in another way, a wave front may be divided up into an infinite number of point sources. The contributions due to this distribution of point sources, when summed together, is then the contribution of the original disturbance source. Today, this same idea is used in numerous branches of engineering and physics (from electromagnetic scattering to digital signal processing), though now it generally goes by the name, *the Superposition Theory*. Superposition theory is applicable to only physical phenomena (such as wave propagation) that are described by *linear partial differential equations*.

Huygens work in physics is so grand that his mathematics is apt to be overlooked. In fact, in the years 1660-1680, he was undoubtedly Europe's greatest mathematician. Newton thought that Huygens is "the most elegant mathematician" of their time. Huygens contributed many elegant results in the infinitesimal calculus leading toward the invention of *calculus*. Related to his work on the pendulum clock, he published the *Huygens' formula*: "The length of an arc of a circle is approximately equal to twice the chord subtending half the arc plus one-third of the

difference between twice this chord and the chord subtending the entire arc." In the theory of numbers, Huygens contributed to the solution of the *Pell* equation. The *Pell* equation was examined by W. Brounker, P. de Fermat, J. Wallis, and L. Euler, and is a *Diophantine* equation of the form:

$$x^2 - r y^2 = 1$$

Here, r is a positive integer, \sqrt{r} is an irrational number, and the unknowns x and y are integers. Huygens' solution to the *Pell* equation involved the use of *continued fraction*, a mathematical technique he pioneered. Let P_s/Q_s ($s = 0, 1, \dots$) be the convergent fractions for the expansion of \sqrt{r} in a continued fraction with period k , then the positive solutions to the *Pell* equation take the form:

$$\text{If } k \text{ is even, } x = P_{kn-1}, \quad y = Q_{kn-1} \quad (n = 1, 2, 3, \dots),$$

$$\text{If } k \text{ is odd, } x = P_{2kn-1}, \quad y = Q_{2kn-1} \quad (n = 1, 2, 3, \dots).$$

For example, since $\sqrt{14} = [3; \overline{1, 2, 1, 6}]$, it follows that the first five convergent fractions of $\sqrt{14}$ are $3/1$, $4/1$, $11/3$, $15/4$, and $101/27$. Since the continued fraction representation of $\sqrt{14}$ has a period of 4, the convergent fraction $[P_{4-1}, Q_{4-1}] = [15, 4]$ provides the first solution of the *Pell* equation $x^2 - 14y^2 = 1$. The next convergent fraction is $[449, 120]$.

Giovanni Domenico (later Jean Dominique) Cassini (1625-1712) was a famous French-Italian astronomer. He discovered four of the eighteen Saturnian moons (Iapetus in 1671, Rhea in 1672, Dione in 1684, and Tethys in 1684). Cassini's most important work concerned the size of the solar system. His published value of the Astronomical Unit (A.U.), the mean distance between the Sun and the Earth was 140 million km. This value is just a few percents lower than today best estimate of 149.5 million km.

Again, Cassini accomplishments in physics and astronomy are so grand that his mathematics is overlooked. In 1680, Cassini studied algebraic curves of the fourth and higher orders. This study was made in connection with his work on the relative motions of the Earth and Sun (in collaboration with Christiaan Huygens and Robert Hooke in 1674). Some of these algebraic curves are now named the "Ovals of Cassini" or the "Cassinian Curve." See Figure 1.

The Cassini oval is described as the locus of a point such that the product of the distances from two fixed points is a constant. These ovals are sometimes called the Cassinian curves, and are described by the following formulae:

$$((x - a)^2 + y^2)((x + a)^2 + y^2) = c^4, \quad a > 0, \quad c > 0.$$

$$\text{Polar coordinates } (r, \phi): r^4 + a^4 - 2r^2 a^2 \cos(2\phi) = c^4.$$

For $c > a$, the Cassinian curve describes a closed curve that has a constriction in the neighborhood of $x = 0$. For $a = c$, the Cassinian curve becomes the Bernoulli lemniscate. For $c < a$, the curve splits into two separate closed curves. Such a unique characteristic of the Cassinian curves has been used to advantage in modeling cell division (however, cell division does not maintain the symmetries found in the mathematical curves) by biologists.

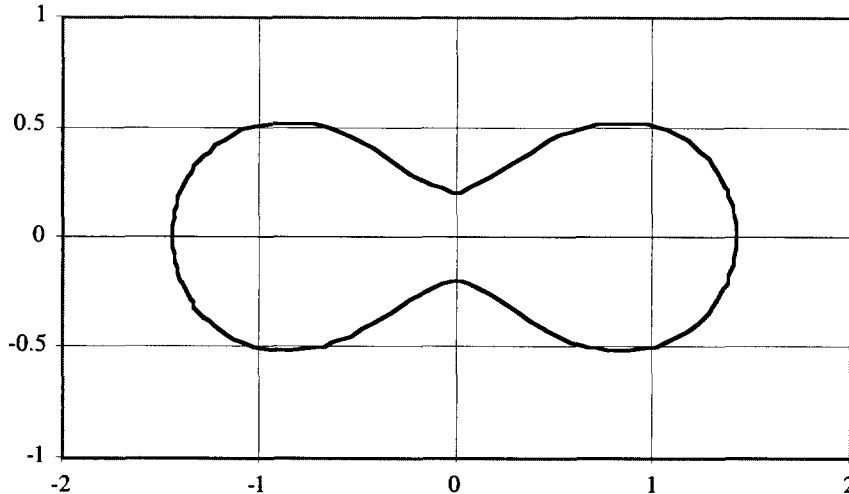


Figure 1. A Cassini "Oval" (Cassinian Curve)

In 1680, Cassini published an interesting result that is related to the Fibonacci numbers: 0, 1, 1, 2, 3, 5, 8, 13, 21, 34, 55, ... In this sequence, each number is the sum of the preceding two. The numbers in the sequence are denoted by F_n , and are formally defined by:

$$F_0 = 0; \quad F_1 = 1; \quad F_{n+2} = F_{n+1} + F_n, \quad n \geq 0.$$

This famous sequence was published in 1202 by Leonardo Fibonacci. The Fibonacci numbers have many interesting properties, one of which is:

$$\lim_{n \rightarrow \infty} \frac{F_{n+1}}{F_n} \rightarrow 2 \cos\left(\frac{\pi}{5}\right) \equiv \text{Golden Ratio}$$

Many artists and writers have said that the *Golden Ratio* is the most aesthetically pleasing proportion and there are many myths that are connected with it. In 1680, Cassini published the elegant identity:

$$F_{n+1}F_{n-1} - F_n^2 = (-1)^n$$

which can be easily proved by induction. It is now named *Cassini's Fibonacci Identity*.

1.4 The Organization of this Paper

This paper is organized as follows. Section 2 gives brief descriptions of the Cassini/Huygens mission to Saturn and Titan as well as the functions of the Attitude and Articulation Control System (AACS). The formulations and solutions of the three Cassini AACS design problems are given in Section 3. Discussions on the philosophy employed and considerations taken in the solutions of these problems are given in Section 4. Conclusions are given in Section 5.

2. CASSINI/HUYGENS MISSION TO SATURN AND TITAN

The Cassini spacecraft was launched on 15 October 1997 by a Titan 4B launch vehicle. After an interplanetary cruise of almost seven years, it will arrive at Saturn in July 2004. To save propellant, Cassini will make several gravity-assist flybys: two at Venus and one each at Earth and Jupiter. Figure 2 shows the interplanetary trajectory design of the Cassini mission.

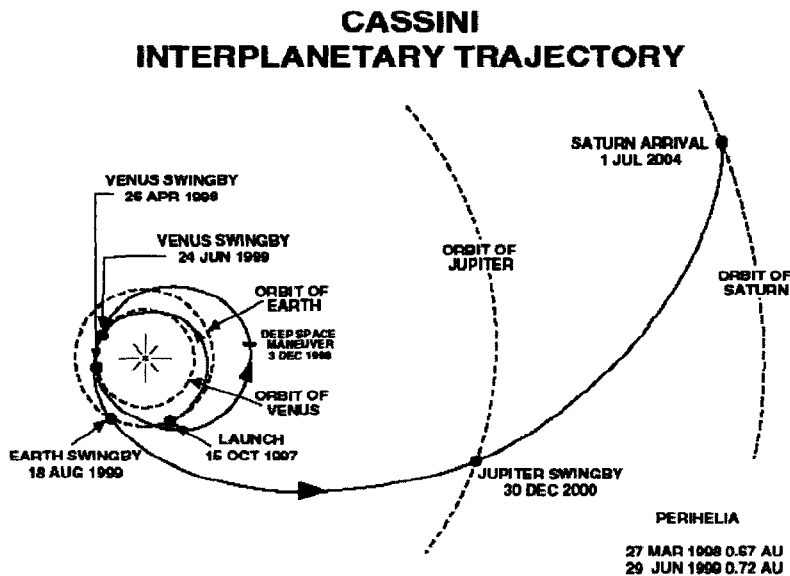


Figure 2. Cassini Interplanetary Trajectory

Unlike Voyagers 1 and 2, which only flew by Saturn, Cassini will orbit the planet for at least four years. Major science objectives of the

Cassini mission include investigations of the configuration and dynamics of Saturn's magnetosphere, the structure and composition of the rings, the characterization of several of Saturn's icy moons, and others. The Huygens probe, developed by the European Space Agency, will be released in December 25, 2004. It will study the atmosphere of Titan, the only moon in the solar system with a substantial atmosphere. Detailed descriptions of various science instruments carried onboard the Cassini spacecraft are given in Ref. 1. Fig. 3 depicts the Cassini spacecraft in its "Cruise" configuration.

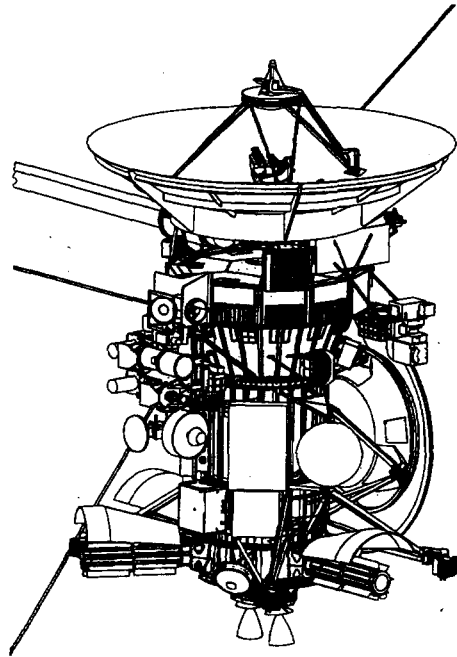


Figure 3. Cassini Cruise Configuration

Cassini's AACS estimates and controls the spacecraft attitude. It responds to ground-commanded pointing goals for the spacecraft's science instrument and/or communication antennas with respect to targets of interest. The AACS also executes ground-commanded spacecraft velocity changes. Hardware that are used by AACS to perform these functions include two attitude control flight computers, an accelerometer, four Reaction Wheel Actuators (RWA), two Sun sensors, two stellar reference units (star trackers), two inertial reference units (each with four sensing axes), and others. This hardware is controlled using on-board flight software algorithms that reside in the flight computers. An overview of the Cassini attitude control algorithm designs is given in Ref. 2.

3. CASSINI ATTITUDE CONTROL SYSTEM DESIGN

3.1 In-flight Estimation of the Cassini Spacecraft's Inertia

Tensor^{3,4}

Several attitude control algorithms onboard the Cassini spacecraft use knowledge of the spacecraft's 3×3 inertia tensor. This tensor is used by both the AACs fault protection algorithms and the attitude estimator. Knowledge of the inertia tensor is also used by the RWA controller that is used to maintain precision spacecraft attitude control during imaging of science targets. As such, a highly accurate estimate of this inertia tensor (matrix) is important.

Before launch, Cassini's inertia tensor was estimated by adding together the moments of inertia of the individual components of the spacecraft. The moments of inertia of individual components were computed with respect to the predicted center of mass of the overall spacecraft before being summed. After launch, the onboard spacecraft inertia matrix is updated periodically using estimates of how much propellant has been used to date, as well as any discrete events (for example, the deployment of the magnetometer boom) that would affect the inertia matrix. The inertia matrix of the spacecraft on March 15, 2000, using the "sum-of-all-components" method, is estimated to be:

$$I_{sc} = \begin{bmatrix} 8810.8 & -136.8 & 115.3 \\ -136.8 & 8157.3 & 156.4 \\ 115.3 & 156.4 & 4721.8 \end{bmatrix} \quad \text{kg-m}^2 \quad (1)$$

This method of calculating the inertia tensor had not been validated against flight estimate using an independent approach until the "conservation of angular momentum" approach that was proposed in Ref. 3.

The underlying principle of the "conservation of angular momentum" approach is explained as follows. When a spacecraft is slewed using the RWAs, the total angular momentum of the spacecraft expressed in an inertial coordinate frame is conserved. This conservation occurs because the addition of angular momentum on the spacecraft due to external torque, such as solar radiation torque, is typically very small over the duration of the slew. Approximate magnitudes of the external torque experienced by the Cassini spacecraft are given in Ref. 4. On March 15, 2000, the largest per-axis external torque due to all sources was about the spacecraft's X-axis, and was less than 1.5×10^{-5} N-m. The conservation of angular momentum allows the total angular momentum evaluated just prior to the beginning of the slew to be set equal to the total angular momentum evaluated throughout the slew. This equality gives an equation for each sample time step throughout the slew with only one unknown: I_{sc} that can then be estimated via a least-squares approach.

Note that I_{SC} contains the moments of inertia of the three stationary reaction wheels.

Over a spacecraft slew, good estimates of the following quantities are available, either from direct measurement prior to launch or from the telemetry data sent down from the spacecraft:

- (1) Spacecraft angular rates (ω_x , ω_y , and ω_z),
- (2) RWA spin rates with respect to its spin axis (ρ_1 , ρ_2 , and ρ_3),
- (3) Spacecraft Euler parameters (q_1 , q_2 , q_3 , and q_4),
- (4) Inertia matrix of the three RWAs (I_{RWA}), and
- (5) Transformation matrix from the RWA spin axes to the XYZ body coordinate frame (T).

The total angular momentum vector of the spacecraft, as expressed in the spacecraft body frame, has two components:

$\vec{H}_{Total} = \vec{H}_{SC} + \vec{H}_{RWA}$. The component due to the spacecraft rates is: $\vec{H}_{SC} = I_{SC}\vec{\omega}$ where $\vec{\omega} = [\omega_x, \omega_y, \omega_z]^T$. To determine the angular momentum of the RWAs, first define $\vec{\rho} = [\rho_1, \rho_2, \rho_3]^T$, where ρ_i is the angular rate of the i^{th} RWA about its spin axis. To find \vec{H}_{RWA} , we simply multiply $\vec{\rho}$ first by the inertia matrix for the RWAs, and then multiply by the transformation matrix T. Note that the component of \vec{H}_{RWA} due to spacecraft rates has already been accounted for in \vec{H}_{SC} .

$$\vec{H}_{RWA} = TI_{RWA}\vec{\rho} \quad (2)$$

The conservation of angular momentum is only valid in an inertial coordinate system. As such, a transformation matrix, P, defined here from the J_{2000} inertial frame to the body coordinate frame, must be defined. It is computed using the four Euler parameters (q_1 , q_2 , q_3 , and q_4). Multiplying the total angular momentum of the spacecraft in body coordinates by the inverse of the transformation matrix P gives the total angular momentum vector in the inertial coordinate frame. The resultant vector, given below, is approximately conserved over a spacecraft slew.

$$\vec{H}_{Total} = P^{-1}I_{SC}\vec{\omega} + P^{-1}TI_{RWA}\vec{\rho} \quad (3)$$

The spacecraft is quiescent just prior to the slew, with all angular rates approximately zero. As such, the initial angular momentum vector is given by:

$$\vec{H}_{Total}(0) = P^{-1}(0)TI_{RWA}\vec{\rho}(0) \quad (4)$$

Invoking the conservation of angular momentum, one gets:

$$P(t)^{-1}I_{SC}\vec{\omega}(t) + P(t)^{-1}TI_{RWA}\vec{\rho}(t) \approx P(0)^{-1}TI_{RWA}\vec{\rho}(0) \quad (5)$$

Now, for the sake of simplicity, consider the special case in which the spacecraft slews about one axis at a time. In this case, the rate components about the other two axes go to zero. For example, for a slew about the X-axis, Eq. (5) becomes:

$$I_{SC} \begin{bmatrix} \omega_x(t) \\ 0 \\ 0 \end{bmatrix} = P(t)P^{-1}(0)TI_{RWA}\vec{\rho}(0) - TI_{RWA}\vec{\rho}(t) \quad (6)$$

Denote the right hand side of Eq. (6) by a new vector. $\vec{Q}(t) = [Q_x(t) \ Q_y(t) \ Q_z(t)]^T$. Using this notation, the first component of the vector-matrix Eq. (6) is: $I_{xx}\omega_x(t) = Q_x(t)$. In Eq. (6), both $\omega_x(t)$ and $Q_x(t)$ will take on a new value for each sample instant, t , throughout the slew, producing a separate equation for each sample instant. If $\vec{\omega}_x$ and \vec{Q}_x represent $N_s \times 1$ column vectors of data points from all sample instances (N_s is the total number of samples), a least-squares approach can be used to find the best estimate of I_{xx} :

$$\hat{I}_{xx} = [\vec{\omega}_x^T \vec{\omega}_x]^{-1} \vec{\omega}_x^T \vec{Q}_x \quad (7)$$

This process can be repeated for I_{yx} and I_{zx} using the pairs of vectors $[\vec{\omega}_x \ \vec{Q}_y]$ and $[\vec{\omega}_x \ \vec{Q}_z]$, respectively. The entire process can then be repeated for slews about the Y and Z-axes as well. This process will give one estimate for each of the moments of inertia and two estimates for each one of the products of inertia (POI). The two POI estimates have been averaged together to obtain the best estimate.

An alternative to the approach described above is to estimate all six independent components of the inertia matrix simultaneously using all the slew data (X, Y, and Z-axis slews) at the same time. The "axis-by-axis" approach described above was used because of its relative simplicity.

At the time when this study was made, only one maneuver had been done with the Cassini spacecraft using the RWAs. This maneuver was done on March 15, 2000 and lasted four hours. The maneuver consisted of a slew about the Y-axis, followed by a slew about the X-axis, another slew about the Y-axis, a slew about the Z-axis, and finally a very small slew about the Y-axis. Telemetry data for the Euler parameters, spacecraft per-axis rates, and RWA spin rates are available over the entire slew duration, at a sample frequency of 0.25 Hz.

The data from March 15, 2000 were analyzed using the proposed methodology. The resulting best estimate for the inertia matrix of the spacecraft was:

$$\hat{I}_{sc} = \begin{bmatrix} 8655.2 & -144 & 132.1 \\ -144 & 7922.7 & 192.1 \\ 132.1 & 192.1 & 4586.2 \end{bmatrix} \text{ kg-m}^2 \quad (8)$$

When compared to the inertia matrix obtained using the existing method (see Eq. (1)), this result validates the existing method, as they are reasonably close. The current results are consistently lower than their counterparts given in Eq. (1) by at most 3%. This offset could point to a bias in the estimate of the spacecraft inertia matrix prior to launch. A bias in the pre-launch estimate is possible because the knowledge requirement for the MOI of the “dry” spacecraft is quite large: $\pm 10\%$. Also, the POI estimates are within 40 kg-m^2 of their counterparts given in Eq. (1). The magnitudes of the POI estimates are all larger than their counterparts given in Eq. (1), which again could be evidence of a bias. Pre-launch, the knowledge requirement for the POI of the “dry” spacecraft is $\pm 75 \text{ kg-m}^2$. The estimation uncertainty matrix associated with \hat{I}_{sc} is derived in Ref. 4.

In conclusion, we note that the least squares estimate of the Cassini spacecraft’s inertia matrix obtained through the conservation of angular momentum method described above agrees closely with that determined by the existing method. This agreement validates the “conservation of angular momentum” method. Using this method, the moments and products of inertia of a spacecraft could be easily estimated whenever telemetry data associated with slewing the spacecraft by the reaction wheels is available.

3.2 Model-based Thruster Leakage Monitor Design⁵

Cassini uses a set of eight thrusters to maintain three-axis attitude control of the spacecraft. Figure 4 shows the locations of the four thruster pods. On each and every one of these pods are mounted two primary thrusters and their “backups.” Pointing controls about the Spacecraft’s X and Y axes are performed using four Z-facing thrusters. Controls about the Z-axis are performed using four Y-facing thrusters. The mono-propellant propulsion system for Cassini is of the blow-down type. With this system, the hydrazine tank pressure, which is $\approx 2550 \text{ kPa}$ at launch, will decay slowly with time as hydrazine is depleted through thruster firings.

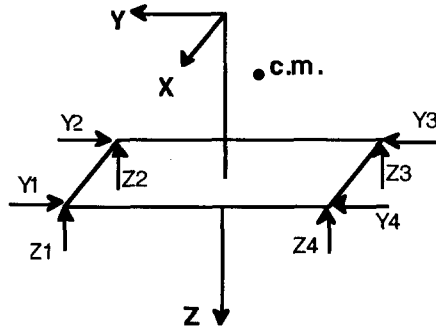


Figure 4. Cassini Thruster Pod Location

If one of the eight prime thrusters leaks, e.g., becomes stuck open, the expelling hydrazine will impart momenta on two of the three spacecraft axes. In response to the resultant attitude control errors that appeared on the affected axes, appropriate thrusters will be fired to maintain the commanded spacecraft attitude. Obviously, the draining of the hydrazine, the excessive firing of the opposing thrusters, and the accumulation of angular momentum on the spacecraft cannot be allowed to persist indefinitely. To protect Cassini against the occurrence of a leaky thruster (an unlikely event), a set of three thruster leak-detection monitors has been designed, tested, and implemented in the flight software.

The main requirement on the thruster leakage-detection monitor design is as follows⁶:

“In the Cruise, Earth approach, and Venus/Earth flyby phases, the attitude control subsystem shall be able to detect any single thruster leak that applied an average torque of at least 0.005, 0.001, and 0.05 Nm, respectively, about any spacecraft axis, and shall isolate the single thruster leak before it applies more than 100 Nms of angular momentum about any spacecraft axis.”

Conventional fault detection methods typically involve the monitoring of one or more of the following quantities: measured system outputs, estimated system states, and estimated process parameters. These measured or estimated quantities are then compared with their nominal values, and their deviations are computed. If any of these deviations persistently exceeds its pre-selected allowable tolerance, an error monitor is triggered to report this abnormality.

This conventional error detection approach is not applicable here because there is not any single measured or estimated quantity that signals the presence of a leaky thruster. A different approach must be taken in designing the thruster leakage monitors. To this end, we first note that the rotational motion of the spacecraft is governed by the following Euler equation:

$$I_{SC}\dot{\vec{\omega}} + \vec{\omega} \times (I_{SC}\vec{\omega} + \vec{H}_{RWA}) = \vec{T}_{RWA} + \vec{T}_{PMS} + \vec{T}_{ENV} + \vec{T}_{LEAK} + \vec{\epsilon} \quad (9)$$

In Eq. (9), I_{SC} is the S/C's inertia tensor. The spacecraft angular rate vector $\vec{\omega}$ is estimated by an onboard attitude estimator. However, it is typically noisy. Hence, the commanded angular rate vector generated by the on-board Attitude Commander is used instead. The spacecraft's angular acceleration vector $\dot{\vec{\omega}}$ is also estimated by the Attitude Commander. Reaction torque exerted on the spacecraft by the reaction wheels, \vec{T}_{RWA} , are estimated onboard by an RWA "manager." Torque exerted on the spacecraft due to thruster firing, \vec{T}_{PMS} , is not available directly. Instead, the on-board propulsion "manager" estimates the force impulse due to all prime thruster firings. Using the estimated thruster moment arms, these force impulses are next converted into three per-axis torque impulses. In effect, what we have estimated is $\int \vec{T}_{PMS}(t)dt$.

Environmental torque due to gravity gradient, solar radiation, magnetic field, atmosphere, etc. is captured in \vec{T}_{ENV} . This torque is typically very small except during planet and Titan flybys. Torque due to a leaky thruster is denoted by \vec{T}_{LEAK} . For example, if the Z_1 thruster leaks, there will be a negative and a positive torque acting on the S/C's X and Y axes, respectively (but with no torque about the Z-axis). Finally, $\vec{\epsilon}$ is used in Eq. (9) to account for both the knowledge uncertainties associated with various S/C's parameters (e.g., inertia tensor) and estimation error associated with various derived spacecraft variables (e.g., thruster momentum impulses).

The error monitor design takes advantage of the fact that the dynamical motion of the spacecraft is governed by Euler's equation. The occurrence of a leaky thruster will impart torque on the spacecraft, upset the "balance" of the Euler's equation. The monitoring of angular momentum that is generated by torque from a leaky thruster is one effective way to detect the presence of a leaky thruster. To this end, let us define the following residual angular momentum vector:

$$\begin{aligned} \vec{R}(t) &= \int_0^t \{ \vec{T}_{LEAK} + \vec{\epsilon} \} dt \\ &= \int_0^t \{ I_{SC} \dot{\vec{\omega}} + \vec{\omega} \times (I_{SC} \vec{\omega} + \vec{H}_{RWA}) - \vec{T}_{RWA} - \vec{T}_{PMS}^f \} dt \end{aligned} \quad (10)$$

Here, \vec{T}_{PMS}^f is a low-pass-filtered version of the noisy raw data and \vec{T}_{ENV} has been neglected in Eq. (10). With no leak, \vec{R} contains only small zero-mean random fluctuations, due to $\vec{\epsilon}$. Whenever a leak appears, two of three \vec{T}_{LEAK} components will be nonzero. If the leak persists, the resultant nonzero components of $\vec{R}(t)$ will grow (either increase or decrease) with time. In time, one of these components will exceed a pre-selected angular

momentum threshold (R_T): $|R_i| \geq R_T$ (where $i = x, y, \text{ or } z$ axis), triggering the error monitor for that particular spacecraft axis. Note that the polarities of R_i (where $i = x, y, \text{ or } z$ axis) reveal the identity of the leaky thruster.

To detect a leak before it imparts more than 100 Nms on any spacecraft axis, we select R_T to be 50 Nms. The rationale for this selection is as follows. The first time the 50-Nms threshold is exceeded, a fault protection activation rule, in attempting to stop the leak, will reset the controller unit for the thruster valve drive electronics. At the same time, all three components of \vec{R} are reset to zero. If the reset of the controller unit does not stop the leak, the same two \vec{R} components will continue to grow with time. The second time the 50-Nms threshold is exceeded, fault protection response will initiate a swapping of the thruster branches, which will stop the leak. In this way, we will be able to stop the leak before it imparts a total of 100 Nms on any spacecraft axis. The selected 50-Nms angular momentum threshold is changeable via command.

3.3.1 Coping with Uncertainties

Not all the uncertainty terms that affect \vec{R} are random in nature. In particular, the thruster-to-thruster variation can impart systematic errors to the Euler equation, causing the \vec{R} components to grow with each thruster firing, even without a leak. As such, prolonged thruster firings could trigger the $|R_i| \geq R_T$ criterion. Two modifications to the described leak detection scheme work to avoid such a false alarm.

First, a correction vector \vec{R}^{Corr} is estimated to account for angular momentum accumulation due to thruster-to-thruster variation. The estimation of the X-axis component of \vec{R}^{Corr} is given here as an illustration. Rotation about the spacecraft X-axis is made using either the Z_1 and Z_2 thruster pair or the Z_3 and Z_4 thruster pair. Hence, the X-axis component of \vec{R}^{Corr} is proportional to both the differential thrusters' impulses and the size of the thruster-to-thruster variation:

$$\begin{aligned} \Delta J_x &= |\Delta J_{Z_3} + \Delta J_{Z_4} - \Delta J_{Z_1} - \Delta J_{Z_2}| \\ R_x^{\text{Corr}} &= 2 \times \eta \times 1.6 \times \Delta J_x \end{aligned} \quad (11)$$

Where ΔJ_{z_j} is the accumulated impulses due to the Z_j thruster over the last sample time. These accumulated impulses are estimated by the onboard propulsion "manager." The thruster-to-thruster variation η is estimated to be 0.05 (i.e., 5%) at launch. If a better estimate is available post-launch, the current value could be updated using the same command that was used to alter R_T . The factor 1.6 represents the average magnitude of the four Z-facing thrusters' moment arms (in meters). The factor 2 is used to account for the standard deviation of a variable that is the sum/difference of four variables, each with a standard deviation of σ , being 2σ . The Y

and Z component of \vec{R}^{Corr} are computed similarly. The correction vector \vec{R}^{Corr} is then added to \vec{R} , and the modified \vec{R} is used in the momentum threshold check.

Next, after the angular momentum threshold is exceeded, a second condition $T_j^{\text{Trigger}} \leq T^{\text{limit}}$, is checked before any fault protection action is initiated. Here, T_j^{Trigger} (j is the spacecraft axis whose $|R_j|$ exceeded R_T) is the time it takes $|R_j|$ to exceed R_T since it was last reset. The T^{limit} threshold is a time-domain threshold that is to be pre-selected. If T_j^{Trigger} is larger than T^{limit} , then we conclude that the threshold was exceeded not because of a thruster leak but is rather due to a systematic accumulation of angular momentum from prolonged thruster firings. On the other hand, if T_j^{Trigger} is smaller than T^{limit} , then there is a real leak, and corrective action from the onboard fault-protection logic is needed. This time domain trigger criterion is illustrated in Figure 5.

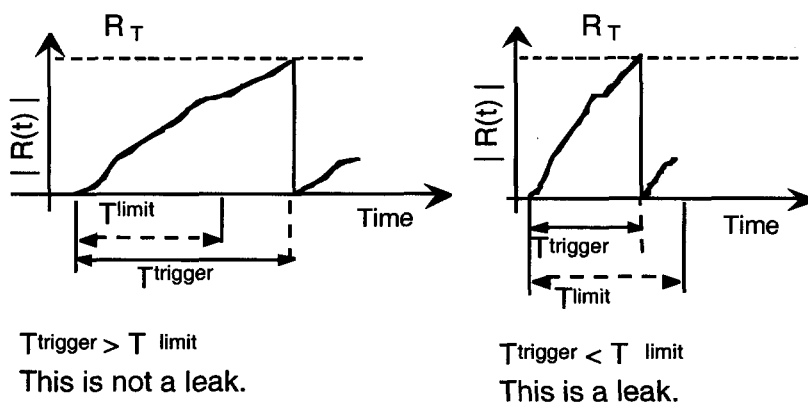


Figure 5. Leak Detection Scheme

For the Cruise phase, we select T^{limit} to be 10 hours. Note that this value is larger than $50/0.005/3600 \approx 2.8$ hours. Hence, the Cruise phase leak detection requirement of 0.005 Nm could be met. Early Cassini flight data indicate that hydrazine is being consumed at a rate of about 1.0 to 1.5 grams per day. This consumption rate is likely to decrease once the spacecraft gets farther away from the Sun. Using a worst-case hydrazine consumption rate of 1.5 grams/day, an upper bound on the per-axis angular momentum (due to thruster-to-thruster variation) that is accumulated over 10 hours is about 0.05 Nms. It is about three orders of magnitude smaller than R_T (50 Nms). As such, the $T^{\text{limit}} = 10$ hours is a good choice for the Cruise phase of the Cassini mission. The time threshold T^{limit} is changeable using the same command that is used to alter R_T . It is to be changed several times throughout the mission to reflect the changing torque detection requirements described above.

3.3.2 Simulation Results

The coded leak-detection error monitor design was tested using the Cassini Flight Software Development Test bed. Attitude control actuators (e.g., thrusters), attitude determination sensors (e.g., gyroscopes), and the spacecraft itself are represented by validated analytical models in this test bed. This test bed can simulate both the pulse-to-pulse and thruster-to-thruster variations, as well as disturbance torque such as that due to a leaky thruster.

The leak-detection monitor is designed to perform its function in many spacecraft scenarios. It must work when the spacecraft is in a quiescent state with its attitude controlled by thrusters (or RWA) as well as when the spacecraft is being slewed about an axis using thrusters (or RWA). As such, its performance in all these scenarios has to be evaluated. In each of these scenarios, test variants that represent combinations of the following conditions must be generated and tested:

- (1) One of the eight prime thrusters is selected as the leaky thruster.
- (2) The leaky thruster is from the prime or backup thruster branches.
- (3) Leakage levels may vary from 0.1 to 100% of the nominal thrust of the thrusters.
- (4) The time at which the leak occurred must also be considered.

A multitude of test variants has to be generated and tested to provide a comprehensive validation of the performance of the thruster leak-detection monitor design. For brevity, only results for a scenario in which the Z_1 thruster develops a 10% leak while the spacecraft is being slewed about the Y-axis are given here (see Fig. 6).

With reference to Fig. 6, we see that a 10% leak in the Z_1 thruster will generate a disturbance torque of -0.158 and $+0.124$ Nm about the S/C's X and Y axes, respectively. This torque will cause the X and Y components of the residual momentum vector to grow with time. About 6 minutes (which is well below T^{limit}) later, $|R_x|$ first exceeded R_T , causing the X-axis error monitor to be triggered. In this particular simulation, we assume that the first corrective action initiated by the fault protection logic (the reset of the controller unit of the thruster valve drive electronics) does not stop the leak. Accordingly, both R_x and R_y will continue to grow with time after having been reset to zero. The next triggering of the error monitor will lead to the swapping of the thruster branches, which stopped the leak.

In this work, a thruster leakage monitor is designed based on the simple fact that a leaky thruster will upset the "balance" of the Euler's equation of motion of the spacecraft. The computational effort involved in executing this set of monitors by the flight computer is moderate. With only two thresholds to select, this set of monitors could be easily managed by Mission Operations controllers. Simulation results indicated that the design meets all the requirements. In particular, the design can detect thruster leaks that are comparable to 0.1% of the thruster magnitude and does so quickly before an unacceptable level of angular momentum is imparted on the spacecraft. The robustness of the design against knowledge uncertainties of various spacecraft parameters as well as

estimation errors of various derived variables has also been confirmed via extensive simulations and five years of flight experience.

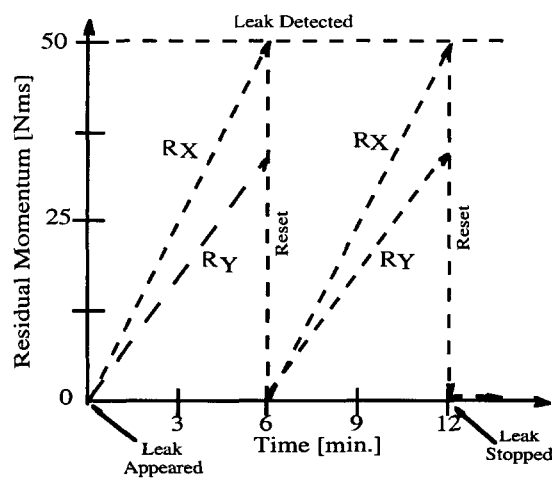


Figure 6. Time Histories of Residual Momentum

3.3 Cassini Pointing System Model^{7,9}

All spacecraft pointing needs could be stated as follow: “align a body vector with an inertial vector.” We call the two vectors involved the “primary” vector pair. This is the fundamental requirement of a pointing goal. However, to uniquely define the spacecraft inertial attitude, the pointing of a second pair of vectors (called secondary vector pair) must also be specified. The spacecraft pointing control system will align the secondary vectors *as close as possible* subjected to the constraint imposed by the primary vector pair.

Inertial pointing of various oriented objects that are mounted on the spacecraft is a central part of spacecraft operations. The pointing system on the Cassini spacecraft serves many “customers.” Examples are the pointing of a science instrument (such as the narrow angle camera) at Saturn, the pointing of the high gain antenna at the Earth, the pointing of the Huygens Probe axis in a pre-determined Probe ejection attitude, and others. In the narrow angle camera example, the primary body vector is the bore sight vector of the camera, which is “fixed” on the spacecraft’s base body. The primary inertial vector is a vector from the spacecraft to Saturn, which varies slowly in time.

The Cassini pointing system is a “general purpose” pointing engine. It accepts generic pointing commands regardless of whether the commands involved are for the purpose of science pointing, antenna pointing, or others. The engine consists of several inter-connected software “objects” working together as a team. Some are collections of

algorithms that run periodically. Others are tables with associated algorithms that run when changes to the tables are commanded. Table 1 and Figure 7 (both are adapted from Reference 7) capture the principal components of the Cassini pointing system design.

Table 1. Principal Components of the Cassini Pointing System Model

Inertial Vector Table	A commandable list of time-varying inertial vectors which are related to one another in a tree topology
Inertial Vector Propagator	Evaluates active members of the Inertial Vector Table
Target Table	A list of paths through the inertial vector tree that are currently needed for target pointing
Target Table Propagator	Evaluates members of the Target Table
Body Vector Table	A commandable list of fixed body vectors
Base Attitude Generator	Evaluates the base attitude for the commanded target
Offset Profile Generator	Evaluates commanded pointing profiles which are offsets relative to the base attitude
Constraint Table	A commandable list of pointing geometric constraints
Constraint Monitor	Detects and corrects violations of constraints by the commanded attitude

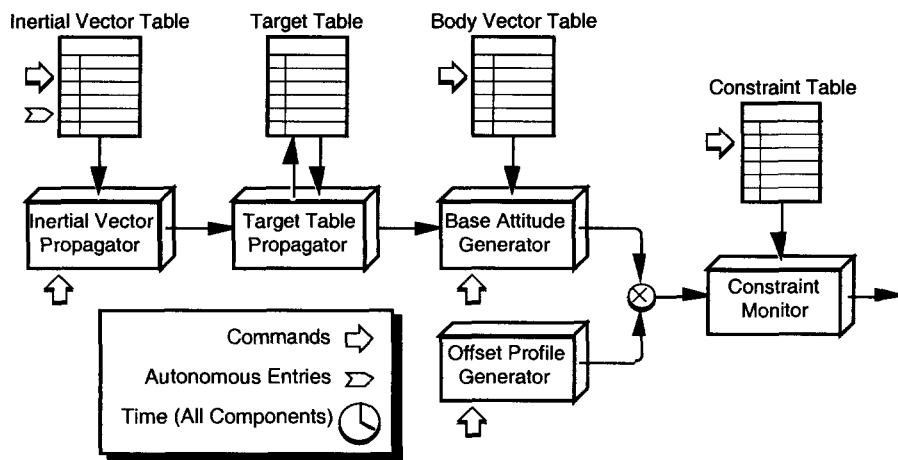


Figure 7. Cassini Pointing System Model⁷

In this paper, for brevity, only the Inertial Vector Propagation (IVP) object is described in details. Readers who are interested in the

details associated with other components of the entire Cassini pointing system model should consult Ref. 7.

Consider the pointing scenario in which we would like to point the narrow angle camera at Saturn. This pointing could be achieved if we have knowledge of the spacecraft-to-Saturn vector in an inertial coordinate frame. This inertial vector could be computed onboard if we have knowledge of the spacecraft and Saturn positions. Hence, we need, in some form, knowledge of the spacecraft trajectory, ephemerides of the planets (for example, Saturn) their moons (for example, Titan), and the motion of target-body features with respect to the target bodies (for example, the predicted landing site of the Huygens probe on the surface of Titan). It will be shown in the following sections that the spacecraft trajectory and the celestial-body ephemerides could be adequately "fitted" by conic sections (called "conics") and Chebyshev polynomials.

As depicted in Fig. 7, three tables are maintained inside IVP. These are the Inertial Vector Table (IVT), the Body Vector Table (BVT) and the Target Table (TT). The IVT stores propagated values of (in general) time-varying inertial vectors. The BVT stores body-fixed unit vectors for various objects (such as the bore sight vector of the camera) identified in the BVT. The TT carries the list of "bases" and "heads" and the information allowing a base-to-head vector to be constructed. Each entry in the table contains two names, one for the object at its head, the other for the object at its base. The remaining data for each entry is a description of the motion of the vector and the time interval over which this description is accurate.

To determine the location of a target from the spacecraft, it may be necessary to follow a path through two or more vectors. During Tour, the Earth is usually found by following a vector path through three tree "branches": spacecraft to Saturn, Saturn to Sun, and Sun to Earth. This path is depicted in Fig. 8. During a close flyby of Titan, the path would contain one more entry: spacecraft to Titan, Titan to Saturn, Saturn to Sun, and Sun to Earth. Once the path to a target is known the vectors along the path are added (with the appropriate sign) to produce the target location.

Most vectors (the arrows in the Fig. 8) could be modeled accurately as conics. Vectors from the Sun to the planets and from the planets to their moons are all well described by conics for long periods of time. When the spacecraft is far from the intersection between spheres of influence of two celestial bodies, conics could also be used to propagate the spacecraft trajectory. Only seven parameters (and time) are necessary to define conics.

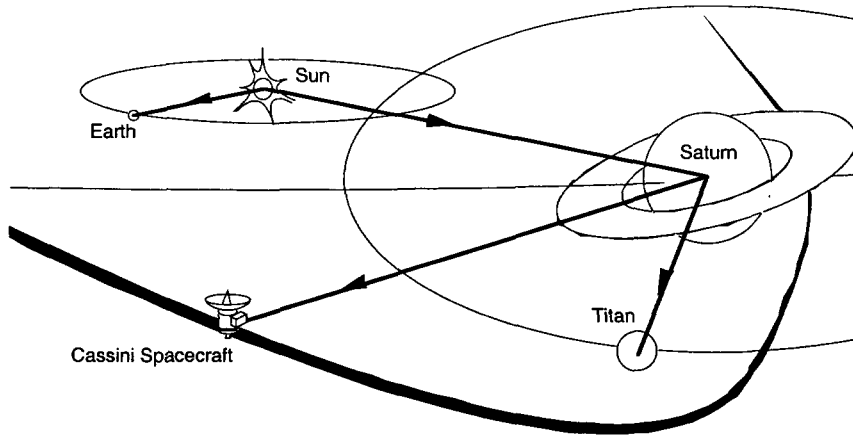


Figure 8. A Representative IVP Vector "Tree" (from Ref. 7)

Because conics do not always suffice, polynomial vectors are also used by the IVP, with each axis up to twelfth order. This propagation approach is not only more expensive (in terms of computational resources), but polynomials also tend not to fit accurately over as long a time interval as do conics. Polynomials will be used mainly to cover transitional periods in the spacecraft's trajectory as gravitational dominance shifts from one body to another. Titan flyby is a frequent example. These two vector propagation approaches are described in details in the following paragraphs.

3.3.1 Conic Background Propagation?

By conics we mean the relative motion which satisfies the differential equation: $\ddot{\vec{r}} = -\mu\vec{r}/|\vec{r}|^3$. Here, \vec{r} is the inertial position vector of the orbiting body relative to the dominant central body and μ is a gravitational parameter (product of the universal gravitational constant G and the sum of the masses of the orbiting and the central bodies). When no other bodies are present the motion $\vec{r}(t)$ follows a true conic (the "Two-body" problem). Perturbing influences of other bodies cause $\vec{r}(t)$ to deviate from a true conic. However, the true motion may still be approximated very well by a series of patched conic where each conic is chosen such that across one segment the deviations of the true path from the conic approximation are kept small.

Conic propagation is really Kepler's problem where given the position \vec{r}_0 and velocity \vec{v}_0 of one body relative to the other at some time t_0 , the position (\vec{r}) and velocity (\vec{v}) are required at some other time t (future or past). A well-known universal formulation proposes the solution to the Kepler's problem as the following nonlinear vector sum:

$$\begin{aligned}\bar{\mathbf{r}}(t) &= F(\bar{\mathbf{r}}_0, \bar{\mathbf{v}}_0, t - t_0)\bar{\mathbf{r}}_0 + G(\bar{\mathbf{r}}_0, \bar{\mathbf{v}}_0, t - t_0)\bar{\mathbf{v}}_0 \\ \bar{\mathbf{v}}(t) &= F'(\bar{\mathbf{r}}_0, \bar{\mathbf{v}}_0, t - t_0)\bar{\mathbf{r}}_0 + G'(\bar{\mathbf{r}}_0, \bar{\mathbf{v}}_0, t - t_0)\bar{\mathbf{v}}_0\end{aligned}\quad (12)$$

$F()$, $F'()$, $G()$ and $G'()$ are time and initial state-dependent scalars whose values depend on the solution of Kepler's equation. Kepler's equation is a transcendental equation and it must be solved iteratively. In the Cassini AACS flight software, Kepler's equation is solved using the Goodyear⁸ algorithm. The Goodyear algorithm was selected because of its robustness, its compactness, and its speed. It never fails to provide a solution. The algorithm solves Eq. (12) in three steps:

[1] Solve the following form of Kepler's equation for the parameter Ψ :

$$(t - t_0) - |\bar{\mathbf{r}}_0| s_1 - \sigma_0 s_2 - \mu s_3 = 0 \quad (13)$$

where :

$$\sigma_0 = \bar{\mathbf{r}}_0^T \bar{\mathbf{v}}_0$$

$$\alpha = \bar{\mathbf{v}}_0^T \bar{\mathbf{v}}_0 - 2\mu / |\bar{\mathbf{r}}_0|$$

$$s_0 = 1 + \alpha\Psi^2/2! + \alpha^2\Psi^4/4! + \alpha^3\Psi^6/6! + \dots$$

$$s_1 = \Psi + \alpha\Psi^3/3! + \alpha^2\Psi^5/5! + \alpha^3\Psi^7/7! + \dots$$

$$s_2 = \Psi^2/2! + \alpha\Psi^4/4! + \alpha^2\Psi^6/6! + \alpha^3\Psi^8/8! + \dots$$

$$s_3 = \Psi^3/3! + \alpha\Psi^5/5! + \alpha^2\Psi^7/7! + \alpha^3\Psi^9/9! + \dots$$

[2] Once Ψ has been evaluated, construct scalars F , G , F' , and G' :

$$\begin{aligned}F &= 1 - \mu s_2 / |\bar{\mathbf{r}}_0| \\ G &= (t - t_0) - \mu s_3 \\ F' &= -\mu s_1 / (|\bar{\mathbf{r}}| |\bar{\mathbf{r}}_0|), \quad \text{where } |\bar{\mathbf{r}}| = |\bar{\mathbf{r}}_0| s_0 + \sigma_0 s_1 + \mu s_2 \\ G' &= 1 - \mu s_2 / |\bar{\mathbf{r}}|\end{aligned}\quad (14)$$

[3] Substitute F , G , F' , and G' in Eq. (12) to arrive at the desired solution.

Note that if only the first terms are retained in the F , G solutions of Eq. (14), Eq. (12) simplifies to: $\bar{\mathbf{r}}(t) = \bar{\mathbf{r}}_0 + (t - t_0)\bar{\mathbf{v}}_0$ and $\bar{\mathbf{v}}(t) = \bar{\mathbf{v}}_0$. This is the degenerate straight-line motion.

3.3.2 Polynomial Background Propagation⁹

When the conic approximation fails to keep the approximation errors small over a reasonable time segment, other means of fitting the

relative position vectors are exercised. Polynomial fits are the logical choice. Among all polynomials, the polynomial with perhaps the most attractive fitting characteristics is the Chebyshev polynomial. The Chebyshev polynomial $T_k(\tau)$ of the first kind is a polynomial in τ of degree k , defined by the relation:

$$T_k(\tau) = \cos(k\theta) \quad \text{where } \tau = \cos\theta \quad (15)$$

We can immediately deduce from Eq. (15) that the first few Chebyshev polynomials are:

$$\begin{aligned} T_0(\tau) &= 1 \\ T_1(\tau) &= \tau \\ T_k(\tau) &= 2\tau T_{k-1}(\tau) - T_{k-2}(\tau), \quad \text{for } k > 1 \end{aligned} \quad (16)$$

Here, τ is the normalized time, which is related to the end-time t_f and the start-time t_s by: $\tau = (2t - t_f - t_s)/(t_f - t_s)$. Chebyshev polynomials can be evaluated recursively using Eq. (16).

Chebyshev polynomials play a pivotal role in the uniform (or ℓ_∞) approximation of functions. They produce the best ℓ_∞ approximation of a time-varying function $f(\tau)$ of ephemeris. The ℓ_∞ -norm (also called the Chebyshev norm) of a fitting error function $e(\tau)$ is defined as:

$$\|e(\tau)\|_\infty = \max_{-1 \leq \tau \leq +1} |e(\tau)| = \max_{-1 \leq \tau \leq +1} \left| f(\tau) - \sum_{i=0}^n C_i T_i(\tau) \right| \quad (17)$$

To fit a time-varying function $f(\tau)$ of ephemeris by Chebyshev polynomials, we must compute coefficients C_i of the expansion $C_0 T_0 + C_1 T_1 + C_2 T_2 + \dots + C_n T_n$ such that for a given "n", the ℓ_∞ -norm given in Eq. (17) is smaller than the 40- μ rad IVP modeling accuracy requirement. Over the time range $|\tau| \leq 1$, the fitting error $e(\tau)$ generated with Chebyshev polynomials attain its absolute maximum value with alternating signs. This is the so-called "equi-oscillation" property. That is, Chebyshev polynomials will distribute the fitting error $e(\tau)$ almost uniformly from one end of a segment to the other. This is a highly desirable feature.

The minimax property is remarkable enough but the Chebyshev polynomials have a second and equally important property, in that they are a family of orthogonal polynomials. That is, they satisfy the following condition:

$$\int_{-1}^1 \frac{T_n(\tau) T_m(\tau)}{\sqrt{1-\tau^2}} d\tau = 0 \quad \text{if } n \neq m \quad (18)$$

Thus the Chebyshev polynomials have an important role in ℓ_2 or least squares approximation too. Its importance among orthogonal polynomials is perhaps only second to the Legendre polynomials.

In the Cassini implementation, we have chosen to fit the three Cartesian position elements (as expressed in an inertial coordinate frame) of the relative position vector between the two points of interest. Three separate fits are required for the three axes and all use the same order polynomial fit (i.e., n is the same for the x , y , and z components). An n - order fit therefore requires $3(n+1)+1$ coefficients to propagate the relative position vector in an inertial coordinate frame. Between these two propagation methods (conics and polynomials), trajectories during the complicated tour can be fit to better than $40 \mu\text{rad}$ (≈ 0.0023 degrees) with only a handful of segments over several weeks. Many entries can be fit accurately enough with a single segment for months or even years.

3.3.3 Conclusions

It must be apparent that quite a few calculations are required to support the Cassini inertial vector propagator. A practical solution to this problem has been found in a multi-tier evaluation system that exploits the smooth variation in most of these vectors. Most of the complicated vector calculations, such as the evaluation of conics, are performed very infrequently. Even for the most rapidly varying trajectory segments we have examined, an update interval of 100 seconds is adequate. Most could be updated much more infrequently and still meet the tightest accuracy requirements. Between updates, they are only interpolated linearly, and then only once per second when the base attitude and its rate are calculated.

The Cassini attitude control algorithms run eight times per second, so the base attitude is actually required at the same rate, but again, this is done by interpolation. The arithmetic necessary to perform these functions is accomplished mostly in a mixture of standard and extended precision MIL-STD-1750 floating point, the latter required primarily for vector calculations. While not ideal, all accuracy requirements have been met with this capability.

4. DISCUSSIONS

4.1 Uses of Physical Laws and Conservation Principles

Physical process is governed by physical law(s). Often times these physical laws lead to conservation principles that should be used to advantage in solving a physical problem.

Unfortunately, unless each and every physical effect that influence the angular motion of a spacecraft is taken into consideration, the angular momentum of the spacecraft, for example, might not be conserved. However, in many physical situations, the conservation principle involved is violated only slightly due to the presence of small disturbance terms. Since relatively small terms in an equation will have

little effect on the solution to that equation, we should investigate whether an approximate application of these conservation principles can still be made. Else, we might miss out an opportunity to greatly simplify the mathematical solution of a physical problem. In the example given in Section 3.1, on the estimation of spacecraft's inertia matrix, we did exploit the conservation of angular momentum principle even though it is held true only approximately.

In Section 3.3, Rasmussen, Singh, Rathbun, and Macala⁷ took advantage of the fact that the motion of a planet (or a spacecraft) under the influence of a dominant central body is *almost* a conic section. But it is only when no other bodies are present that the motion of an object follows a true conics. But this did not stop us from using the conics because the on-board implementation of a "more" exact solution is likely to be prohibitively expensive. The approach taken then is to limit the use of conics to both Cruise and Tour scenarios in which they fit the actual trajectory very accurately. However, during a close encounter with Titan, when the spacecraft is under the influence of both Saturn and Titan, the conic approximation can introduce unacceptably large error. In these scenarios, alternative mathematical treatments such as the uses of high-order polynomials (which are relatively more computational intensive) become necessary.

The assertion that relatively small terms in an equation will have little effect on the solution to that equation is often true, but is not true in general. To be certain, one should perform a few "spot" checks of the effects of the neglected terms on the solution of the problem. In the case of inertia tensor estimation, the solar radiation torque might be small but it isn't constant (due to the changing spacecraft attitude). Nevertheless, we can still incorporate a representative constant solar radiation torque into Eq. (6) in our estimation of the spacecraft's inertia tensor. If the resultant change in the estimated inertia tensor is larger than the desired estimation accuracy, then one might want to consider the inclusion of this second-order effect in the estimation process.

4.2 Exact Solutions: They are Expensive and Unnecessary

A mathematical model of a physical situation is often a simplified description of many complex physical effects involved. Model simplifications must be made if there is any hope of solving the resultant problem formulated. One way to simplify a physical situation is to obtain informal estimates of the numerical significance of various physical effects that affect the physical situation. After obtaining the required estimates it then makes sense to simply remove the relatively small terms from the mathematical model.

Knowing that the mathematical model is just an approximate description of the physics involved, does it then make sense to find an *exact* solution to this *approximately* formulated model? The answer is *No* especially when the exact solution is *expensive*. By expensive we meant it is costly to find that exact solution (in both time and money). We also meant that the exact solution might require the use of hard-to-measure or hard-to-estimate data input. The implementation of an exact solution that

requires the uses of unavailable computer CPU time and memory is also not possible. Not all of these constraining factors apply in any specific situation but it is rare for a number of them not to apply. In this regard, one prefers an approximate solution that is good enough because it satisfies all the applicable accuracy requirements (see Section 4.3). The on-board implementation of a solution method that achieves significantly better than the requirement is a waste of the limited on-board computing resources and is unnecessary.

4.3 A Model is Good if it meets All Applicable Requirements

To answer the question on whether a particular approximation solution to a formulated problem is adequate we must first define what is “adequate.” An approximate solution is adequate if it satisfies all the applicable requirements. We will use the 40- μ rad IVP accuracy requirement as an example to illustrate the process.

The Cassini spacecraft carries science cameras that are charge-coupled-device imager. These “staring” sensors have “electronic” shutters that snap open quickly so that all parts of the frame are exposed at the same time. For these science instruments, science pointing control requirements are commonly selected to be smaller than one-third the size of the field of view (FOV) of the imaging sensor. In so doing, one can be certain that the science target is captured inside the picture frame. For the Cassini spacecraft, the narrow angle camera has a FOV of 6.2 milliradians ($1^\circ \approx 17.45$ mrad). The pointing control requirement for science pointing is 2 mrad (radial 99%).⁶

Table 2. Cassini Science Pointing Control Error Budget

Error Sources	3σ (mrads)	
	X-axis	Z-axis
Attitude determination error	0.22	0.06
Star tracker geometric distortion error	0.56	0.035
Post-calibration misalignment between camera and star tracker boresight vectors	1.0	0.1
Star tracker boresight vector shift between calibrations	0.2	0.2
Reaction wheel-based attitude control error	0.04	0.04
IVP timing error	0.037	0.037
IVP modeling error	0.04	0.04
Root-Sum-Squares	1.18	0.23
Capability (radial 99%)	1.03	
Requirement (radial 99%)	2.00	

To assess whether we can meet this pointing control requirement, a system engineer must build an error budget such as that shown in Table 2. Since the camera is aligned with the spacecraft’s Y axis, only the pointing errors associated with the spacecraft’s X and Z axes are considered in Table 2. There are altogether seven pointing error sources.

Some of these errors are large (such as the star tracker geometric distortion error) and others are small (such as the IVP modeling error). Together, the overall pointing capability of the spacecraft, 1.03 mrad, is significantly better than the pointing control requirement (2.0 mrad, 99% radial). Hence, there just isn't any compelling reason to tighten the IVP modeling error requirement from its current allocation of 40 μ rad to a smaller number. As such, knowing that the Goodyear algorithm can meet the 40- μ rad accuracy requirement, no other "better-than-requirement" algorithms to the Kepler's problem need to be considered.

4.4 Manipulation of A Model into A Responsive Form

A model may have been formulated with perfect propriety but it is almost always a mistake to jump in with an extensive series of computations using that model. Instead, it is better to live with it for a bit, to view it from different angles, and mould it into a form that is more "responsive" to the problem that we want to solve.

In Section 3.2, we note that the spacecraft angular motion is governed by Euler's equation. The presence of a leaking thruster will introduce a non-zero \vec{T}_{LEAK} term on the right hand side of Eq. (9). However, any attempt to compute \vec{T}_{LEAK} using the following equation will encounter difficulty:

$$\vec{T}_{LEAK} = I_{SC}\dot{\vec{\omega}} + \vec{\omega} \times (I_{SC}\vec{\omega} + \vec{H}_{RWA}) - \vec{T}_{RWA} - \vec{T}_{PMS} - \vec{T}_{ENV} - \vec{\epsilon} \quad (19)$$

This is because the "size" of \vec{T}_{LEAK} could be as small as $0.1\% \times 1 N \times 1.234 m \approx 1.234 \times 10^{-3} Nm$. It is larger than the magnitude of \vec{T}_{ENV} but it is smaller than that of $\vec{\epsilon}$. As such, the non-zero \vec{T}_{LEAK} term due to a leaking thruster will be "buried" in the "noise" generated by $\vec{\epsilon}$. Any attempt to detect thruster leakage via the monitoring of Eq. (19) will be difficult.

To overcome this difficulty, we took advantage of the following two physical facts. Firstly, a thruster leak will introduce a persistent \vec{T}_{LEAK} term. As such, while its magnitude might be small, but over a long period of time, the angular momentum accumulated due to \vec{T}_{LEAK} will be sizable and detectable. Secondly, the angular momentum accumulation due to zero-mean random fluctuations $\vec{\epsilon}$ will be small (the presence of any systematic errors is taken care of in Section 3.3.2). Hence, it is easier to detect the presence of a rising angular momentum vector instead of the presence of a small leak-induced torque. Therefore, we transformed the original Euler's equation (Eq. (9)) into the angular momentum equation (Eq. (10)) which is more "responsive" to the problem we want to solve.

4.5 Iterative Refinements of A Model

A mistake commonly made by engineers is their attempts to incorporate a long list of physical effects in the model created to solve a physical problem. The result of such an approach is usually confusion and frustration. It is almost always more practical to start by choosing one or a few dominant effects and creating a model which accounts for these effects only. When such a model has been created and evaluated, it is much easier to add other secondary effects to this “backbone” model in an incremental refinement process.

The thruster leakage-detection monitor design described in Section 3.2 is such a “backbone” model. It has captured the most dominating physical effect involved, the Euler’s equation of motion of a rigid body. In Section 3.2.1, effects on Eq. (10) due to various secondary factors such as the thruster-to-thruster and pulse-to-pulse variations of the thruster magnitude were considered. Judgement was then used in the incorporations of some of these secondary effects in the model. The resultant refined model will be robust against these variations but might be harder to use. The refinement process is stopped when the final model is usable (i.e., it meets all applicable requirements) for the purpose in hand.

5. CONCLUSIONS

In this paper, the mathematical treatments of three engineering problems related to the Cassini spacecraft attitude and articulation control system designs are described. Common among these mathematical treatments is our emphasis on the need to have a good understanding of the underlying physical principles that governed the physical processes involved. In all cases, these understandings led us to simple yet adequate solutions to seemingly complex engineering problems. Also, we emphasized the need to establish a set of clearly defined requirements for the problem. These requirements represent clear “targets” that the engineers could use to judge whether the solution in hand is good enough. A sophisticated algorithm that generates “better than requirement” solution is a waste of resources. Both Huygens and Cassini are preeminent mathematicians who had mastered the art and science of applying mathematics to the solutions of physical problems. In all cases, they introduced relatively simple mathematical models for describing complicated physical situations. Within the models introduced, they drawn ingenious conclusions from the mathematical solution and elaborated their consequences by means of advanced mathematics. When it is combined with a good understanding of the physics involved, and in the hands of trained engineers, mathematics is indeed a powerful tool in solving “real-life” engineering problems.

6. ACKNOWLEDGEMENTS

The research described in this paper was carried out by the Jet Propulsion Laboratory, California Institute of Technology, under a contract with the National Aeronautics and Space Administration. The author is grateful to Dr. Robert Rasmussen, Dr. Gurkirpal Singh, and Miss Julie Wertz, his colleagues at Jet Propulsion Laboratory, for helpful discussions.

7. REFERENCES

1. Jaffe, L., and Herrell, L., "Cassini Huygens Science Instruments, Spacecraft, and Mission," *Journal of Spacecraft and Rockets*, Vol. 34, No. 4, 1997, pp. 509-521.
2. Wong, E., and Breckenridge, W., "An Attitude Control Design for the Cassini Spacecraft," *Proceedings of the AIAA Guidance, Navigation, and Control Conference*, AIAA, Washington, DC, 1995, pp. 931-945.
3. Lee, A.Y. and Wertz, J. "Inflight Calibration of the Cassini Spacecraft Inertia Matrix," *Journal of Spacecraft and Rockets*, Vol. 39, No. 1, pp. 153-155, January-February, 2002.
4. Wertz, J. and Lee, A.Y., "Inflight Estimation of the Cassini Spacecraft's Inertia Tensor," *Proceedings of the 11th AAS/AIAA Space Flight Mechanics Meeting*, Santa Barbara, California, Feb. 11-15, 2001.
5. Lee, A.Y., "Model-based Thruster Leakage Monitor for the Cassini Spacecraft," *Journal of Spacecraft and Rockets*, Vol. 36, No. 5, pp. 745-749, September-October, 1999.
6. Walker, J.W. and Lee, A.Y., "Cassini Orbiter Functional Requirement Book: Attitude and Articulation Control Subsystem," CAS-4-2007, Revision F, JPL D-699-205, November 1997. Jet Propulsion Laboratory, California Institute of Technology.
7. Rasmussen, R.D., Singh, Gurkirpal, Rathbun, D.B., and Macala, G.A., "Behavioral Model Pointing on Cassini Using Target Vectors", *Advances in the Astronautical Sciences*, Volume 88, AAS 95-006. See also SPIE Vol. 2803, pp. 271-287.
8. Goodyear, W. H., "Completely General Closed-Form Solution for Coordinates and Partial Derivatives of the Two-Body Problem", *The Astronomical Journal*, Vol. 70, No. 3, April 1965, pp. 189-192.
9. Singh, Gurkirpal, "Cassini Inertial Vector Propagation Algorithms," Section 6 of the *Cassini Control Analysis Book*, PD 699-410, JPL D-9638, November 12, 1998. Jet Propulsion Laboratory, California Institute of Technology.